International Journal of Nanomedicine

Dovepress
Taylor & Francis Group

Open Access Full Text Article

ORIGINAL RESEARCH

Polydopamine Modified with Brain Targeting Peptide Rabies Virus Glycoprotein for Treatment of Alzheimer's Disease by Inhibiting Oxidative Stress and Inflammatory Response

Heling Chu[1,*], Yihao Sun[2,*], Chuyi Huang[3,*], Lei Wang[4], Qihao Guo[1,*], Lixian Jiang[5,6,*]

[1]Department of Gerontology, Shanghai Sixth People's Hospital Affiliated to Shanghai Jiao Tong University School of Medicine, Shanghai, People's Republic of China; [2]Department of General Practice, Shanghai Sixth People's Hospital Affiliated to Shanghai Jiao Tong University School of Medicine, Shanghai, People's Republic of China; [3]Health Management Center, Renji Hospital, School of Medicine, Shanghai Jiaotong University, Shanghai, People's Republic of China; [4]Department of Orthopedic Surgery, Shanghai Sixth People's Hospital Affiliated to Shanghai Jiao Tong University School of Medicine, Shanghai, People's Republic of China; [5]Shanghai Key Laboratory of Neuro-Ultrasound for Diagnosis and Treatment, Shanghai Sixth People's Hospital Affiliated to Shanghai Jiao Tong University School of Medicine, Shanghai, People's Republic of China; [6]Department of Ultrasound in Medicine, Shanghai Sixth People's Hospital Affiliated to Shanghai Jiao Tong University School of Medicine, Shanghai, People's Republic of China

*These authors contributed equally to this work

Correspondence: Lixian Jiang, Shanghai Key Laboratory of Neuro-Ultrasound for Diagnosis and Treatment, Shanghai Sixth People's Hospital Affiliated to Shanghai Jiao Tong University School of Medicine, No. 600, Yishan Road, Shanghai, 200233, People's Republic of China, Email jianglixian958@outlook.com; Qihao Guo, Department of Gerontology, Shanghai Sixth People's Hospital Affiliated to Shanghai Jiao Tong University School of Medicine, No. 600, Yishan Road, Shanghai, 200233, People's Republic of China, Email qhguo@sjtu.edu.cn

Purpose: Polydopamine (PDA) has been recognized as an antioxidant and anti-inflammatory agent. However, the difficulty to cross blood-brain barrier (BBB) limits PDA's neuroprotective effects in the brain. Here, we aimed to construct PDA-rabies virus glycoprotein (RVG) by modifying the RVG29 polypeptide on PDA nanoparticles (NPs) and investigate whether PDA-RVG improved the cognitive function and pathology of Alzheimer's Disease (AD) by inhibiting oxidative stress and inflammatory response.

Methods: We prepared and characterized PDA NPs and tested whether PDA improved AD pathology in APP/PS1 mice. To facilitate PDA's penetration across BBB, we modified RVG29 on PDA and examined its brain-specific targeting ability and biocompatibility. We further tested the effects of PDA-RVG on oxidative stress, inflammatory response and ferroptosis in both in vitro and in vivo AD models.

Results: PDA demonstrated robust reactive oxygen species (ROS)-scavenging activity and effectively reduced Aβ deposition and the expression of APP and PS1 in APP/PS1 mice. PDA-RVG successfully crossed BBB in an in vitro BBB model. Meanwhile, compared with PDA, PDA-RVG intravenous injection exhibited good brain-specific targeting ability. Moreover, the hematological analysis revealed no significant differences between the PDA-RVG and control groups. In the in vitro AD experiment, PDA-RVG reduced ROS, inducible nitric oxide synthase, and pro-inflammatory cytokines levels in BV2 cells. Besides, PDA-RVG decreased ROS and apoptosis, while increased glutathione peroxidase4 (GPX4) and the viability of PC12 cells. More importantly, intravenous delivery of PDA-RVG improved cognitive function assessed by Morris water maze, and upregulated the ferroptosis-protective proteins Ferritin Heavy Chain 1 and GPX4 expression, while PDA alone did not lead to cognitive improvement.

Conclusion: PDA reduces AD pathology, which is possibly attributed to its ability to scavenge ROS, ameliorate the inflammatory microenvironment and inhibit ferroptosis. Intravenous delivery of PDA-RVG has good brain-specific targeting ability and biocompatibility, and improves cognitive function in AD mice. This study provides a safe, effective, and promising therapeutic strategy for AD via oxidative stress-associated target.

Keywords: Alzheimer's disease, polydopamine, PDA-RVG, oxidative stress, neuroinflammation, ferroptosis

https://doi.org/10.2147/IJN.S564013
Received: 19 September 2025
Accepted: 22 January 2026
Published: 5 February 2026

Introduction

Alzheimer's disease (AD), as the leading cause of dementia, accounts for 60% to 80% of cases. AD and related dementias contribute significantly to progressive decline in daily activities among older adults.[1,2] The extracellular accumulation and aggregation of amyloid-β (Aβ) and intracellular neurofibrillary tangles, which are composed of hyperphosphorylated tau, are the neuropathological hallmarks of AD.[3,4]

In spite of unremitting efforts, there are still limited effective therapeutic options for AD. Recent trials of disease-modifying therapies targeting Aβ, such as donanemab and lecanemab, show promise in slowing cognitive and functional decline.[5,6] However, these treatments are costly and associated with specific adverse effects, which indicates an investigation of additional treatment avenues is warranted.[7] The disturbance of the balance between the overproduction of reactive oxygen species (ROS) and the cellular antioxidant defense system is called oxidative stress, which is considered as a key contributor to the evolution of AD.[8] Oxidative stress is considered as an early crucial central factor in the pathogenesis of AD, which may lead to Aβ deposition and tau protein dimerization and its subsequent hyperphosphorylation.[9,10] Ferroptosis, characterized as an iron-dependent regulated necrosis resulting from extensive lipid peroxidation-induced membrane damage, represents the cell death modality most intricately linked to oxidative stress.[11] More importantly, ferroptosis is related to AD pathogenesis via multiple mechanisms.[12] Accordingly, the antioxidant and anti-ferroptosis therapies may provide new approaches to discovering and developing novel anti-AD drugs.

Dopamine, an endogenous nitrogenous organic compound, represents the predominant catecholamine neurotransmitter in the human brain.[13] Clinically, dopamine is widely used to treat various diseases such as Parkinson's disease, renal failure, and ischemic shock.[14] Dopamine monomers self-assemble into polydopamine (PDA), which gains broad biomedical application due to its excellent biocompatibility and biodegradability.[15] PDA serves as an antioxidant capable of inhibiting inflammatory responses and oxidative stress.[16] It can eliminate ROS through redox reactions, radical trapping, and hydrogen atom transfer.[17] The properties of PDA-its small particle size, modifiability, and biocompatibility-make it particularly advantageous for treating brain disorders, especially those characterized by prominent oxidative stress and neuroinflammation such as AD.[18] Previous study has demonstrated that PDA nanoparticles (NPs) reduce neuroinflammation in AD model.[19]

However, about 98% of small molecule drugs and nearly 100% of macromolecular drugs cannot penetrate the blood-brain barrier (BBB) to access brain tissue.[20] It has been reported that PDA has poor brain-targeting ability.[21] Thus, enabling PDA NPs to effectively target to the brain and exert its biological effects remains challenging, which always requires the assistance of a drug delivery system. Rabies virus glycoprotein 29 (RVG29), a 29-amino acid peptide derived from RVG, exhibits unique specificity for binding to nicotinic acetylcholine receptors (nAChRs) in the brain.[22] This binding triggers receptor-mediated transcytosis, enabling the drug to easily penetrate the BBB and enter the brain.[23,24] Correspondingly, the modification with RVG29 peptides nanomedicines facilitates their entry to the brain and binding to nAChR on the surface of endothelial cells. During subsequent endocytosis, this complex is encapsulated in endosomal vesicles, taken up by endothelial cells, and released into brain tissue through intricate transport pathways.[25] This property endows RVG29 significant advantages in drug delivery systems, which enables more effective delivery of drugs, nucleic acids, and NPs into neurons. Previous studies have revealed that RVG29 enables nanomedicines to penetrate BBB and act on neurons in AD treatment.[26,27] In addition, RVG29 has been used to assist PDA in targeted delivery to brain in ischemic stroke.[28]

We first studied whether PDA NPs decreased AD pathology in this study. Then we constructed PDA-RVG by modifying the RVG29 polypeptide on its surface to enhance its brain-targeting efficacy. We further investigated whether PDA-RVG improved the cognitive function by ROS clearance, inflammation inhibition, and ferroptosis reduction.

Materials and Methods

Materials

Dopamine hydrochloride and NH_2-PEG-COOH (Mw=2000 Da) were purchased from Shanghai Ponsure Biotech, Inc. Dulbecco's modified Eagle medium (DMEM), trypsin, and fetal bovine serum (FBS) were purchased from Gibco. Ammonia, $FeCl_2$, and 1,10-phenanthroline were purchased from Macklin Biochemical Co., Ltd., and 1-ethyl-3-(3-(dimethylamino) propyl) carbodiimide (EDC) and N-hydroxysuccinimide (NHS) were from Sigma. The reagents/kits used for biological

analyses were fluorescein isothiocyanate (FITC, Aladdin Holdings Co., Ltd)., calcein-AM/PI (Dojindo Co., Ltd)., erastin (MedChemExpress), 3,3′-diaminobenzidine (DAB, TCI Co. Ltd)., C11 BODIPY (GlpBio Technology, Inc)., Cell Counting Kit-8 (CCK-8, Beyotime Institute of Biotechnology Co., Ltd)., 2, 7-dichlorodihydrofluorescein diacetic acid (DCFH-DA) (Beyotime Institute of Biotechnology Co., Ltd). The ELISA kits were purchased from Neobioscience Technology Co, Ltd. FITC-Dextran (40 kD), Acriflavine and Rhodamine B (RhB) were purchased from Adamas-beta. Fluorimetric Fluorescamine Protein Quantitation Kit was purchased from AAT Bioquest.

Synthesis of PDA NPs and PDA-RVG NPs

Normal PDA NPs were synthesized in an alkaline solution. 10 mL of water was used to disperse 0.5 g of dopamine hydrochloride, which was then added to a mixture of distilled water (90 mL) and ethanol (40 mL). The ammonia solution (2 mL) was then added and agitated for a whole day. The reaction product was centrifuged at 15000 rpm for 15 minutes to obtain a precipitate, which was washed 3 times with deionized water.

The following protocol was used to obtain the RVG29-modified PDA. NHS/EDC (100 mM) was used to activate the PDA NPs. Then an equimolar amount of NH_2-PEG-COOH was added to the PDA NPs solution in five aliquots, followed by 2 hours of stirring the mixture. Unreacted NH2-PEG-COOH and NHS/EDC were removed by centrifugation. After re-suspending the precipitate, the RVG29 solution was added and stirred for 2 hours. The solution was repeatedly washed with distilled water for further analysis.[29] The peptide quantitation of RVG29 was performed as Supplementary Method 1.

Characterization of the PDA NPs and PDA-RVG NPs

After dropping PDA and PDA-RVG NPs solution onto a copper mesh, we collected transmission electron microscopy (TEM) images of the NPs using a TEM operated at 80 kV to examine the morphology and structure. The NPs' hydration particle size and zeta potential were evaluated by dynamic light scattering (DLS) using a Zetasizer Nano ZS (Malvern Instruments Ltd., Worcestershire, UK) (Supplementary Method 1).

ROS Scavenging Tests

The electron spin resonance (ESR) spectrum (ESR 5000, Bruker, Germany) was used to study the ability of PDA and PDA-RVG to scavenge the hydroxyl radical (·OH) and hydroperoxyl radical (·OOH). 5,5-dimethyl-1-pyrroline-Noxide (DMPO) (5 μL; 10 mM) served as the trapping agent and was dissolved in phosphate buffer saline (PBS) (45 μL; 10 mM) in a typical assay. Subsequently, Fe^{2+} (20 μL; 50 mM) was added to catalyze the production of ·OH from H_2O_2 (30 μL; 50 mM). The amount of ·OH was quantified based on the intensity of the ESR amplitude. Meanwhile, superoxide anions ($\cdot O_2^-$) was produced by adding 70 μg of KO_2 into 200 μL of the 18-crown-6 in dimethyl sulfoxide (DMSO) solution (0.7 mM) and then trapped by DMPO (50 μL). The ESR performance, with or without adding NPs, was evaluated to determine the superoxide dismutase (SOD)-like enzyme activity of PDA and PDA-RVG.

Verification of Fusion

The fusion of PDA and RVG29 polypeptide was investigated using the Förster resonance energy transfer (FRET) method. In this section, two dyes were used: Acriflavine and RhB. After adding these dyes separately into PDA and RVG29 polypeptide, RVG29 polypeptide in various ratios (5:1, 3:1, 2:1, and 1:1) was mixed with PDA and amide condensation for 3 hours. The fluorescence spectra of each sample from 500 nm to 650 nm was measured using a Tecan Spark20M microplate reader after excitation at 460 nm. The five microliters of fused PDA-RVG suspension on a glass slide with glycerol gelatin were fixed to further validate the fusion. A simple physical mixture without a fusion process was used as a control. Fluorescence images were obtained using a fluorescence microscope (A1s, Nikon, Japan).

Cell Culture

The Chinese Academy of Science Cell Bank was the source of the PC12 and BV2 cell lines. BV2 and PC12 cells were cultured in DMEM (Gibco) supplemented with 10% FBS (Gibco) and 1% penicillin-streptomycin (PS, Gibco). All cells were kept in a humidified incubator at 37°C and 5% CO_2. To establish the in vitro AD model, BV2 and PC12 cells were

treated with Aβ42 of 20 μM. The cells were randomly divided into control, Aβ42, Aβ42+PDA and Aβ42+PDA-RVG groups.

In vitro BBB Penetration Assay

In vitro BBB model was established as previous report.[30] 2×10^5 b.End3 cells were seeded into a Transwell chamber with a filter diameter of 2.0 μm, and the whole was placed in a 12-well plate and incubated at 37 °C for 24 hours. The culture medium in the upper chamber was replaced 0.5 mL daily, while 1.5 mL of culture medium in the lower chamber was replaced every 2–3 days. The tight connectivity of the BBB was verified by measuring the transendothelial electrical resistance (TEER) of the co-cultured model using a Millicell ERS instrument to ensure 100% cell confluence (Supplementary Method 1). Also, the BBB permeability assays were performed as Supplementary Method 1.

The chamber was transferred to a culture plate inoculated with PC12 cells and the 12-well plate was equilibrated at 37 °C for 1 day. The Transwell chamber was filled with 20 μL of PDA or PDA-RVG NPs at a concentration of 1 mg/m, which were then put in the incubator. After 4 hours, the cells were washed with PBS, fixed with 4% paraformaldehyde, and stained with the nuclear marker DAPI, followed by further observation under a laser confocal microscope.

Animals

Male C57/BL6-Tg transgenic mice (APP695swe/PSEN1-dE9, APP/PS1) aged 9 months were purchased from Shanghai Model Organisms Center, Inc. Mice were kept in a 12 h/12 h light-dark cycle with free access to food and water under standard laboratory conditions (temperature: 22 ± 2°C; humidity: 40%). The mice were randomly divided into control (sham operation), PDA, and PDA-RVG groups. Sham-operated mice were subjected to the same procedure while only normal saline of equal dose was injected.

The mice were euthanized by cervical dislocation in accordance with American Veterinary Medical Association (AVMA) guidelines. Our animal studies were conducted in accordance with the Guideline for Ethical Review of Animal Welfare published by China (GB/T 35892–2018), and were approved by Institutional Animal Care and Use Committee of Shanghai Sixth People's Hospital Affiliated to Shanghai Jiao Tong University School of Medicine (No. 2024–0239).

Drug Injection

Isoflurane was used to anesthetize the mice via a mask (3% for induction, 1.5% for maintenance in 70% nitrous oxide and 30% oxygen). PDA was dissolved in normal saline to prepare a solution with a concentration of 1 mg/mL. PDA solution of 6 μL was intracerebroventricularly injected at the rate of 2 μL/min with a stereotaxic frame at 1.0 mm lateral to the midline, 0.5 mm posterior to the coronal suture and at a depth of 1.5 mm from the surface of the brain. The tests were performed at 1 d, 3 d and 7 d after PDA intracerebroventricular injection. PDA-RVG was also prepared into a 1 mg/mL solution. Different from PDA, PDA-RVG was injected intravenously at the dose of 100 μL daily for 20 consecutive days, after which the measurements were performed. All mice were put into the cage for keeping warm after drug injection.

Brain-Specific Targeting Study of PDA-RVG in APP/PS1 Mice

APP/PS1 mice were injected with sulfated cyanine 5.5 (Cy5.5)-labeled NPs (PDA and PDA-RVG). All the NPs were adjusted to carry an equal fluorescent intensity and delivered to the mice via tail vein injection. The fluorescence in the brain was quantified using a live imaging device at 1, 2, 6, 12, and 24 hours after injection. Then the mice were sacrificed, and the brain was divided into five equal parts along the coronal plane.

Biocompatibility Evaluation of PDA-RVG

The safety of PDA-RVG was further evaluated in vivo. PDA-RVG was intravenously administered into the mice (n=5) every other day for one week. The body weight was recorded. Blood samples were collected for the purposes of hematological and hemochemical analysis.

Intracellular ROS Assessment

Cells from different treatment groups were incubated with 10 μM DCFH-DA (Reactive Oxygen Species Assay Kit, Beyotime, S0033M) for 20 minutes at 37°C. After incubation, the cells were washed three times with PBS to remove excess DCFH-DA, followed by further examination under a fluorescence microscope (BZ-X810, Keyence, Japan).

Immunohistochemistry

At 3 days after PDA injection, APP/PS1 mice (n=4) were anesthetized. Subsequently, they were perfused with normal saline solution followed by 4% ice-cold paraformaldehyde via the left cardiac ventricle. The brain tissues were then removed and underwent gradient dehydration. Serial coronal sections with a thickness of 10 μm were cut using a freezing microtome, and the sections were blocked with 10% goat serum after washing. The sections were incubated overnight at 4 °C with an anti-$A\beta_{1\text{-}42}$ rabbit polyclonal antibody (1:500, Abcam, Cambridge, UK). Then, they were incubated for 1 h at 37 °C with horseradish peroxidase (HRP) coupled secondary goat anti-rabbit IgG (1:500, Abcam).[31]

For quantitative Aβ plaque counting, six non-overlapping fields per coronal section in the ipsilateral or contralateral cortex were randomly selected under high-power magnification (×400). The mean value across these fields was defined as the Aβ plaque count. Field selection was conducted by an investigator blinded to group assignments.

Immunofluorescence

BV2 and PC12 cells underwent fixation using 4% paraformaldehyde (30 min), subsequent permeabilization with 0.1% Triton X-100 (10 min), and final blocking with 5% goat serum albumin (BSA) (30 min). The cells were incubated overnight at 4°C with anti-inducible nitric oxide synthase (iNOS) and anti-glutathione peroxidase4 (GPX4) rabbit polyclonal antibodies (1:500, Abcam), followed by incubated with FITC labeled goat anti-rabbit secondary antibodies (1:500, Abcam) for 1 hour at 37°C. Afterwards, the stained cells were examined using a fluorescence microscope (BZ-X810, Keyence, Japan).[32]

Enzyme-Linked Immunosorbent Assay (ELISA)

The concentrations of different inflammatory cytokines including interleukin-1β (IL-1β), IL-6, and tumor necrosis factor-α (TNF-α) were determined by ELISA. The supernatant from BV2 cell cultures was collected and stored at −80°C to prevent protein degradation. According to the manufacturer's instructions, the cytokine concentrations were measured using a double-antibody sandwich ELISA kit, and absorbance was measured at 450 nm using an automated microplate reader.

Apoptosis Assays

PC12 cells were seeded into 6-well plates, and after 12 hours, apoptosis was examined. Immediately afterward, the cells were treated with 20 μM Aβ42 for 8 hours and co-cultured with the NPs. An annexin V-FITC/ propidium iodide (PI) apoptosis detection kit was applied to detect apoptosis in the cell samples in accordance with the manufacturer's instructions. The fluorescence intensity was examined with flow cytometry (NovoCyte Adv, Agilent, USA).

Live/Dead Cell Staining Imaging

For the live/dead staining, PC12 cells were seeded into 6-well plates and cultured for 12 hours. After treated with 20 μM Aβ42 for 8 hours, the viability of the PC12 cells in each group was confirmed with the Calcein-AM and PI staining kit according to the instructions of manufacturer. The fluorescence images were obtained via a fluorescence microscope.

Western Blot

The cortex tissues were homogenized and the Western blot was performed as our previous report.[33] Anti-amyloid precursor protein (APP) (1:1000, Abcam), anti-presenilin1 (PSEN1) (1:1000, Abcam), anti-Ferritin Heavy Chain 1 (FTH1) (1:1000, Abcam), and anti-GPX4 (1:1000, Abcam) rabbit polyclonal antibodies were used as primary antibodies. Glyceraldehyde 3-phosphate dehydrogenase (GAPDH) functioned as an internal control.

Quantitative Real-Time Polymerase Chain Reaction (qRT-PCR) Analysis

Total RNA was extracted from the cortical tissue using Trizol Reagent (Sigma-Aldrich, St Louis, USA). Then, the PrimeScript^{TM} RT reagent kit (Takara, Shiga, Japan) was used to reverse-transcrib RNA from each sample was to cDNA. Using an ABI PRISM 7500 system (Applied BioSystems, Waltham, USA), the qRT PCR was carried out via a SYBR Green Master Mix (TaKaRa, Japan). The mRNA expression levels were normalized to GAPDH gene using the $2^{-\Delta\Delta}$CT method.[34] Table 1 included the sequences of the primers.

Morris Water Maze (MWM) Test

Spatial learning and memory were assessed via MWM test following established protocols.[35,36] A black circular pool (120 cm diameter × 60 cm height), divided into four quadrants, contained water maintained at 25±2°C. Multiple extra-maze cues were observable from the pool area, likely serving as spatial orientation references for the mice. The cues kept a fixed spatial position during the entire experiment. A 10-cm-diameter escape platform was placed 2 cm beneath the water surface in the target quadrant. Mice were assigned to random entry points in four water quadrants and subjected to a five-day training protocol for submerged platform navigation. Each of these 5 days consisted of 4 trials with 2-minute inter-trial intervals. Mice were given 60 seconds to find the platform. They were guided to the platform and allowed to spend 10 seconds on the platform in case of the failure to find the platform. Mice were then patted dry with a cloth and put back into a warm cage after each trail. For data analyses, a latency time of 60 seconds was assigned to mice that failed to reach the platform without guidance. The formal test was conducted at day 6, in which the mice were allowed a maximum of 180 seconds. After 3 tests were completed, the average score was recorded. The video tracking system (Dig-Behav, Jiliang Co. Ltd., Shanghai, China) automatically calculated the latency to reach the platform, the distance traveled, and the swimming speed. Each group contained 5 mice and the observers were blinded to the groups.

Rotarod Test

Rotarod test was performed by using a Rotarod apparatus (IITC Life Science, Woodland Hills, USA) to test the motor coordination and balance of mice. Before testing, mice were habituated and pretrained on the Rotarod (15 rpm) for 5 minutes over 3 days. On the test day, mice were subjected to a rotarod trial starting at 4 rpm and accelerating linearly to 40 rpm over 300 seconds; their latency to fall was recorded. Each mouse was tested over 3 trials with 15-minute intervals between trials, and then the average latency to fall was recorded.[37]

Statistical Analysis

All data were presented as mean ± standard deviations after a normal distribution test was performed. Statistical analysis was carried out using SPSS22.0. Depending on the number of groups, either a two-tailed Student *t* test or one-way analysis of variance (ANOVA) was employed for statistical comparisons. When ANOVA indicated significant differences, Tukey's honestly significant difference (HSD) test was used for intergroup comparisons. Student *t* test was used to compare the differences of hematological and hemochemical parameters, Western blot and qRT-PCR analysis of FTH1 and GPX4 between control and PDA-RVG groups. ANOVA followed by Tukey's HSD test was used for comparison among the groups in Aβ plaque counting, Western blot and qRT-PCR analysis of APP and PSEN1, immunofluorescence

Table 1 Primer Sequences Used for qRT-qPCR

Gene	Forward Primer (5′-3′)	Reverse Primer (5′-3′)
App	GCAATGATCTCCCGCTGGTA	AACTTTGGGTTGACACGCTG
Psen1	TGGAGACTGGAACACAACCA	AATGGCGAGCAGGAGTAATG
Gpx4	CAGGAGCCAGGAAGTAAT	CAGCCGTTCTTATCAATGAG
Fth1	GCCGAGAAACTGATGAAGCTGC	GCACACTCCATTGCATTCAGCC
GAPDH	AGGTCGGTGTGAACGGATTTG	TGTAGACCATGTAGTTGAGGTCA

analysis in BV2 and PC12 cells, ELISA analysis for inflammatory cytokines, MWM test, and Rotarod test. The statistical significance level was defined as $P<0.05$. GraphPad Prism 9.00 software was utilized for figure creation.

Results

Preparation, Characterization, and Multiple Enzyme-Mimicking Activities of PDA

In this study, PDA NPs with ROS scavenging ability were successfully prepared using classical methods. After stirring for 24 hours, dopamine self-polymerized into PDA NPs in an aqueous solution containing ethanol and ammonia. TEM imaging was performed to determine the morphological features and particle size distribution of PDA NPs (Figure 1A and B). TEM images showed the successful synthesis of PDA NPs, with uniform particle size distribution and an average size distribution of approximately 100 nm to 120 nm. According to the high-angle annular dark field (HAADF) images and associated area-elemental mappings, C, N, and O elements coexisted in the prepared PDA NPs (Figure 1C). DLS analysis revealed that the PDA particle size was 154.90 ± 0.99 nm, and the zeta potential was approximately −35.86 ± 0.49 mV, indicating good drug stability (Figure 1D).

As mentioned above, the pathological process of AD disease is greatly impacted by oxidative stress and neuroinflammation triggered by excessive ROS. Effectively scavenging excessive ROS to restore a normal microenvironment is crucial for alleviating AD pathology. Therefore, we investigated the scavenging capability of PDA on typical ROS, such as ·OH and $\cdot O_2^-$. The generator of ·OH was the system of Fe^{2+} with H_2O_2. The characteristic peak intensity of ·OH/DMPO at a ratio of 1:2:2:1 was reduced significantly with unique operations. Meanwhile, with the administration of PDA, there was a reduction in the peak intensity of ·OH in a concentration-dependent manner (Figure 1E). In the 18-crown-6/DMSO solution, the $\cdot O_2^-$ generated by the ionization of potassium superoxide was captured by DMPO to form DMPO-OH, which exhibited

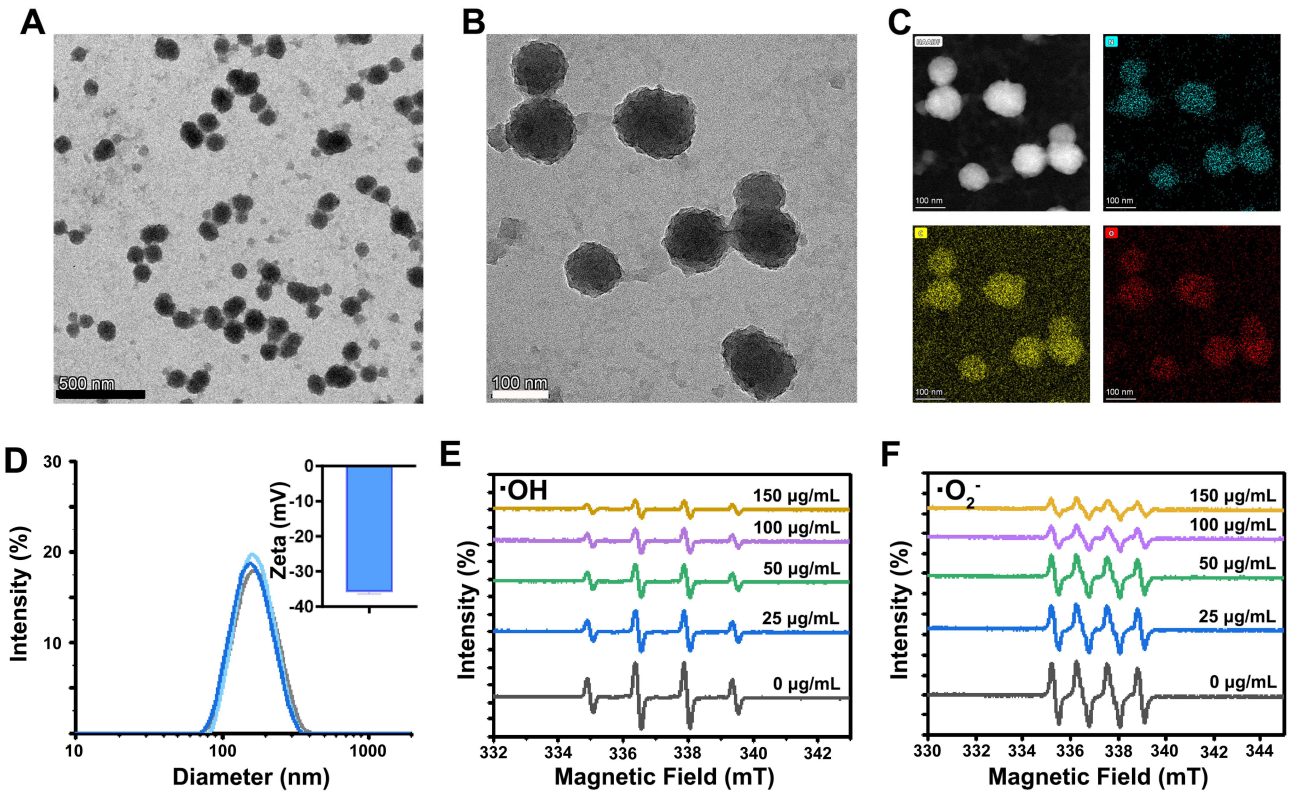

Figure 1 Characterization and ROS enzyme-mimicking ability of PDA NPs. (**A** and **B**) TEM images of PDA NPs, scale bar: 500 nm and 100 nm. (**C**) High-angle annular dark-field images and associated area-elemental mappings of PDA NPs, with the images of HAADF, N, C, and O elements, respectively, Scale bar: 100 nm. (**D**) Size distribution analysis and zeta potential of PDA NPs. (**E** and **F**) Electron paramagnetic resonance curve of the scavenging activated oxygen, including ·OH (**E**) and $\cdot O_2^-$ (**F**), with DMPO as the spin trap. The values of Y-axis were not displayed as all the curves were plotted in a single graph to clearly present the details and differences of the curves.

https://doi.org/10.2147/IJN.S564013

a 1:1:1:1 signal peak in the ESR spectrum. The intensity of the ($\cdot O_2^-$) peak was decreased by PDA, suggesting that PDA can scavenge ($\cdot O_2^-$) and the scavenging ability increases with increasing concentration. (Figure 1F).

The Effect of PDA on Aβ Deposition in APP/PS1 Mice

Immunohistochemistry showed that Aβ plaques in the ipsilateral and contralateral cortex were reduced at 3 day after intracerebroventricular injection of PDA ($P<0.05$). Notably, Aβ staining was further decreased in the ipsilateral cortex than in the contralateral cortex ($P<0.01$) (Figure 2). It indicated that PDA alleviated AD pathology, and a better effect was observed in the brain region closer to the injection site.

The Effect of PDA on AD-Related Proteins in APP/PS1 Mice

Western blot revealed that APP protein was decreased at 1 day after PDA intracerebroventricularly injected and maintained decreasing during 7 days ($P<0.001$) (Figure 3A). A down-regulation trend in the *App* gene was also observed after PDA was injected, and the statistical difference was observed at 3 days ($P<0.05$) (Figure 3B). Similarly, PDA reduced PSEN1 protein at 3 days and 7 days, and the *Pesn1* gene was decreased at 3 days after PDA administration ($P<0.05$) (Figure 3C and D).

Preparation, Fabrication, and Multiple Enzyme-Mimicking Activities of PDA-RVG

The morphology of centrifugally purified PDA-RVG was directly observed using TEM. As shown in Figure 4A, the particles exhibited regular spherical shapes with uniform distribution and no obvious adhesion. The average particle size and distribution of PDA-RVG were determined by DLS measurement, which showed the average particle size was 172.37 ± 1.66 nm, and the size distribution of the PDA-RVG was unimodal, indicating the formation of the expected monodisperse NPs (Figure S1A). Zeta-potential analysis revealed a significant increase from −35.86 ± 0.60 mV for bare PDA to −21.63 ± 1.62 mV for PDA-RVG following RVG29 conjugation (Figure S1B). This positive shift is consistent with the successful presentation of the cationic peptide, which was further quantified at a density of 18.13 μg of RVG29 peptide per mg of PDA (Figure S1C).

As shown in Figure S1D and E, Fourier transform infrared (FTIR) spectroscopy was employed to provide direct chemical evidence for the successful conjugation of RVG29 to the PDA NPs. The FTIR spectra clearly exhibited the appearance of several characteristic absorption bands that were absent in the spectrum of bare PDA, forming a robust evidence chain for successful immobilization. Specifically, we observed: (i) the emergence of the Amide I band at

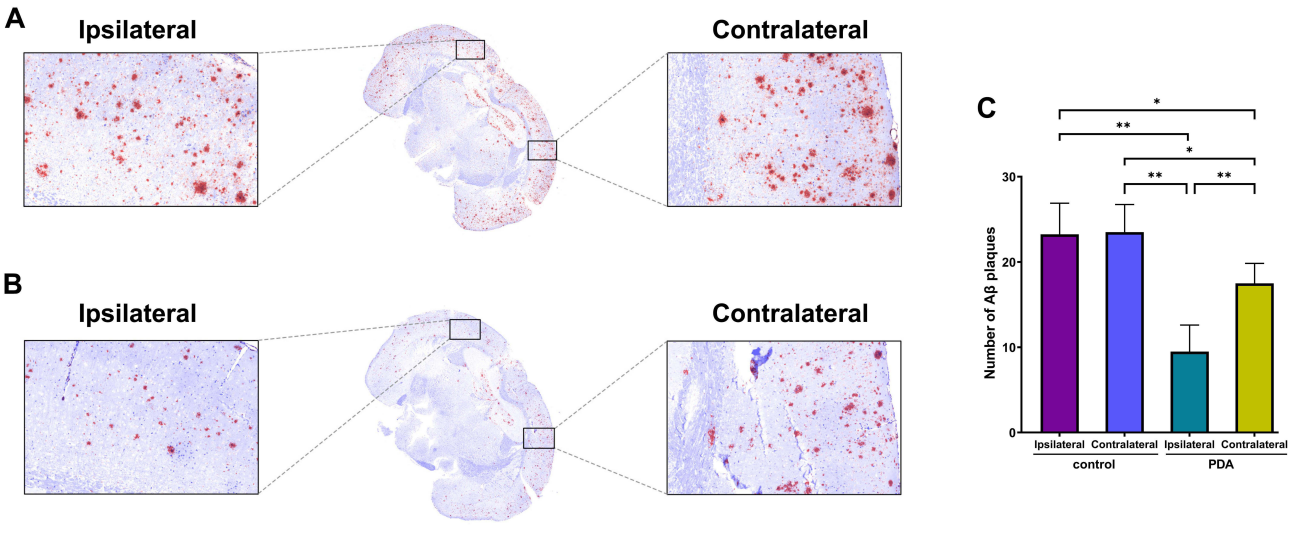

Figure 2 The effect of PDA on Aβ deposition. It was shown in immunohistochemistry and quantitative analysis that Aβ plaques in both ipsilateral and contralateral cortex were reduced at 3 d after intracerebroventricular injection of PDA compared with the control group. (**A**) control group; (**B**) PDA group; (**C**) quantitative analysis; *$P<0.05$, **$P<0.01$.

https://doi.org/10.2147/IJN.S564013

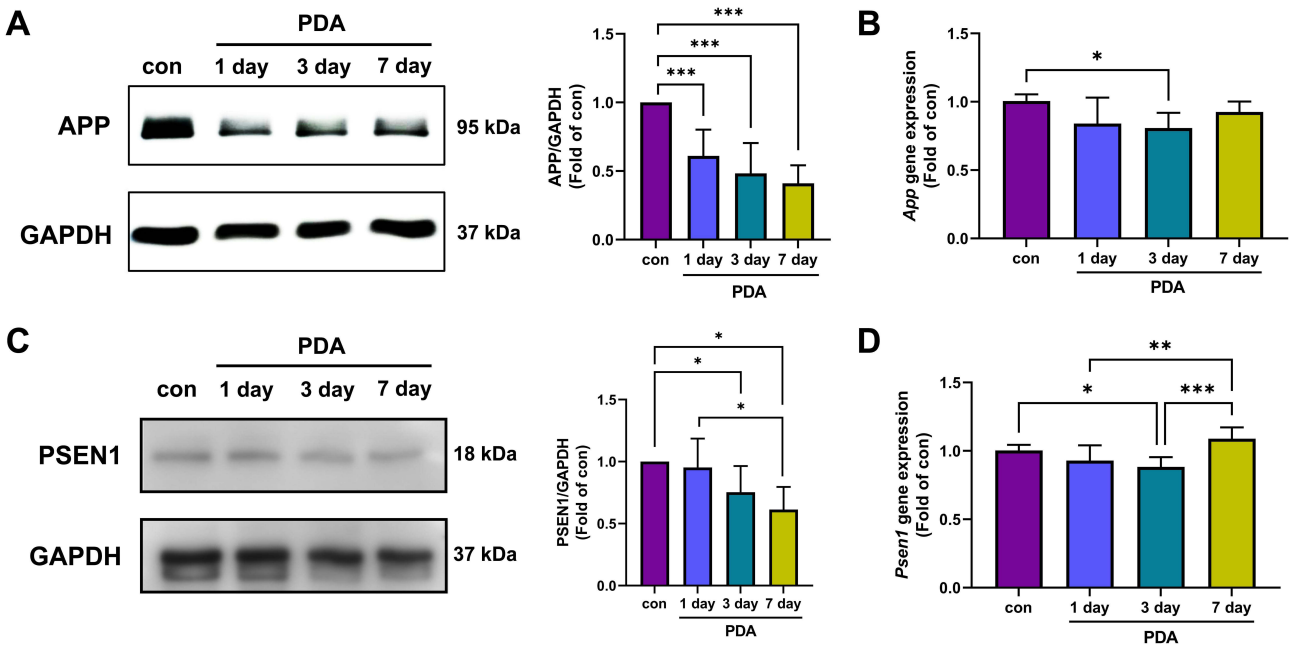

Figure 3 The effect of PDA on the expression of APP and PSEN1. Western blot revealed that APP protein decreased at 1 day after PDA intracerebroventricular injection and lasted 7 days (**A**). *App* gene was down-regulated at 3 days after PDA injection (**B**). Similarly, PSEN1 protein was reduced by PDA at 3 days and 7 days (**C**). The *Pesn1* gene was decreased at 3 days after PDA administration, while it appeared to have a "rebound" increase at 7 days (**D**). **P*<0.05, ***P*<0.01, ****P*<0.001.

~1650 cm^{-1} and the Amide II band at ~1540 cm^{-1}, confirming the presence of the peptide backbone on the PDA surface; (ii) distinct new peaks at ~1200 cm^{-1} and ~1140 cm^{-1}, which served as a unique fingerprint for the guanidyl group of the arginine residues within the RVG29 sequence; and (iii) a new peak at ~1400 cm^{-1}, attributed to the symmetric stretching of carboxylate ions (COO^-) from the aspartic acid and/or glutamic acid residues of the peptide. The collective presence of these RVG29-specific peaks unequivocally verified the successful conjugation of the peptide onto the PDA NPs.

To verify the successful modification of RVG29 polypeptide on the surface of PDA, we used two different dyes to label PDA and RVG29 polypeptide, forming a FRET pair. When the two fluorescent dyes were in close proximity, the energy generated by Naphtalimide (NBD) (at 520 nm) can be transferred non-radiatively to RhB, resulting in excitation light at 580 nm. By mixing PDA and RVG29 polypeptide in different proportions and covalently binding them through amide condensation, we applied excitation light at 460 nm to the sample. We detected the emission intensity in the range of 500–650 nm. Compared with the use of PDA-NBD alone, the addition of RVG29-RhB and covalent binding increased fluorescence intensity at 580 nm and decreased at 520 nm, indicating the most significant FRET effect. When PDA-NBD and RVG29-RhB were physically mixed in equal proportions without covalent binding through amide condensation, no significant fluorescence emission peak was observed at 580 nm (Figure 4B, blank line). This may be due to the significant shortening of the distance between PDA and RVG29 polypeptide caused by covalent bonds, leading to energy transfer from PDA-NBD at 520 nm to RVG29-RhB, which produced excitation light at 580 nm. In addition, under fluorescence microscopy, compared with the red and green fluorescence separation exhibited by simple physical mixing of PDA and RVG29 polypeptide, PDA-RVG exhibited superimposed yellow fluorescence (Figure 4C). In summary, the above results confirm the successful encapsulation of RVG29 polypeptide in PDA.

More importantly, the decrease of the intensity of ·OH by PDA-RVG was similar to that by PDA, which in turn verified that the RVG29 polypeptide hardly affected the catalytic performance (Figure 4D). The capability of PDA-RVG to scavenge $\cdot O_2^-$ was also detected through the application of ESR analysis. The ESR findings revealed that PDA-RVG significantly lowered the intensity of $\cdot O_2^-$ with a ratio of 1:1:1:1 (Figure 4E). That is, PDA-RVG has a superior SOD activity.

https://doi.org/10.2147/IJN.S564013

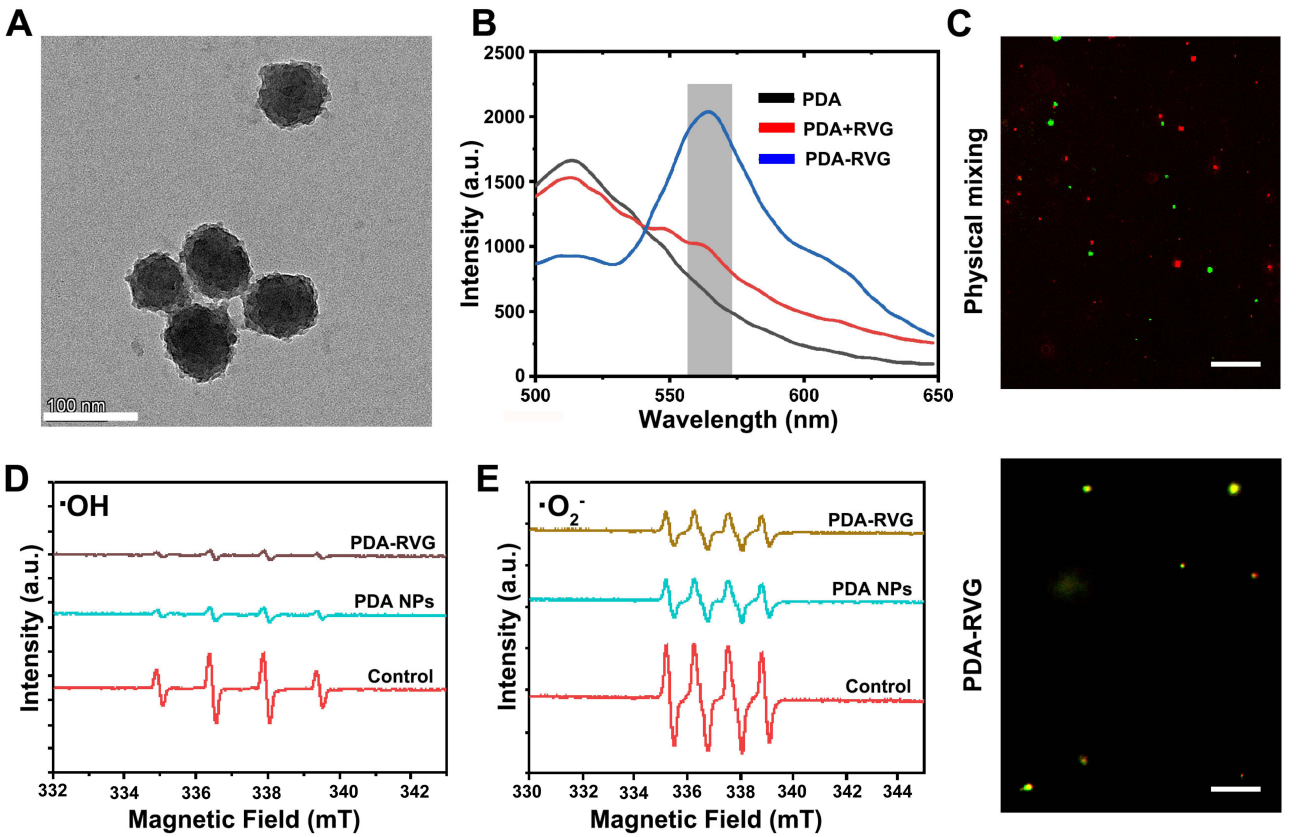

Figure 4 Characterization and ROS enzyme-mimicking ability of PDA-RVG NPs. (**A**) TEM images of PDA-RVG NPs, scale bar: 100 nm. (**B**) PDA (Naphtalimide) fused with increasing RVG29 polypeptide (RhB), and the fluorescence spectrum was recorded. (**C**) Confocal fluorescence images of PDA-RVG and a physical mixture of PDA and RVG29 polypeptide (green: PDA; red: RVG29 polypeptide; Scale bar: 10 μm). (**D** and **E**) Electron paramagnetic resonance curve of the scavenging activated oxygen including ·OH (**D**) and $\cdot O_2^-$ (**E**), with DMPO as the spin trap. The values of Y-axis were not displayed as all the curves were plotted in a single graph to clearly present the details and differences of the curves.

Brain-Specific Targeting Ability and Biocompatibility Evaluation of PDA-RVG

An in vitro BBB model was constructed using Transwell chambers to investigate the ability of PDA-RVG modified by RVG29 polypeptide engineering to cross the BBB. The integrity of the in vitro BBB model was rigorously validated. The TEER values increased over time, stabilizing at a plateau of approximately 220 $\Omega \cdot cm^2$, indicative of a tight cell monolayer (Figure S2A). This was complemented by a dextran-FITC permeability assay, which showed no significant paracellular diffusion of the tracer after 7 days in culture (Figure S2B). Together, these data confirmed the formation of a functional endothelial barrier, providing a validated model for the subsequent assessment of NP penetration.

PDA-RVG was added to the small chamber, and the fluorescence content of PDA-RVG in PC12 cells in the outer chamber was detected after 24 hours (Figure 5A). PDA was used as a control. As shown in Figure 5B, compared with PDA, the modification with RVG29 polypeptide exhibited more fluorescence accumulation in PC12 cells, indicating that RVG29 polypeptide modification can impart the ability of PDA-RVG to cross the BBB, which was beneficial for its delivery through the intravenous drug delivery system to the brain of AD mice.

We further examined the brain-targeting ability of PDA-RVG and its biodistribution in vivo. First, we intravenously injected Cy5.5-labeled PDA and PDA-RVG and then performed in vivo brain-specific targeting ability on APP/PS1 mice at different time points (1 hour, 2 hours, 6 hours, 12 hours, and 24 hours) after treatment. The fluorescence signal of Cy5.5 was detected in the brain 1 hour after injection, gradually increased over time with a peak at 6 hours and lasted at least 24 hours (Figure 5C). It is worth noting that much higher fluorescence intensity in the brain was observed in Cy5.5-PDA-RVG group than Cy5.5-PDA group with broader fluorescence expression at all five time points. Moreover, to confirm the presence of PDA-RVG in the brain, brain tissue was removed 24 hours after injection and divided into five

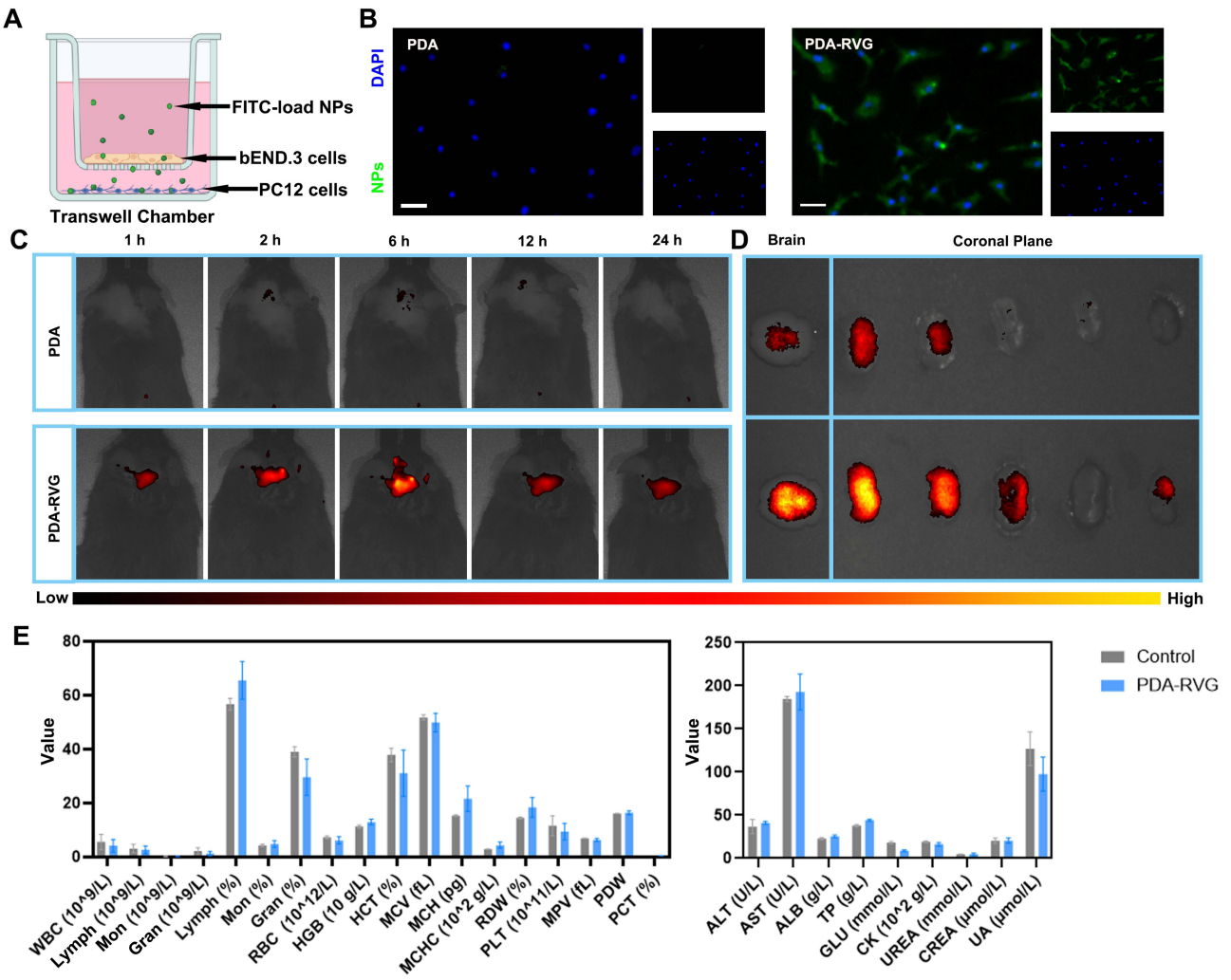

Figure 5 Brain-specific targeting ability and biocompatibility evaluation of PDA-RVG. (**A**) Schematic showing the application of PDA-RVG and the in vitro model of the BBB with b.End.3 cells and PC12 cells for permeability studies. (**B**) Representative photomicrographs of FITC-load PDA and PDA-RVG in PC12 cells showed that PDA-RVG exhibited more fluorescence accumulation compared with PDA. The larger image represents merge of the right two smaller images including NPs (Green) and DAPI (Blue). Scale bar: 50 μm; (**C**) Representative in vivo imaging system (IVIS) images of AD mice demonstrated that higher fluorescence intensity in the brain was observed in Cy5.5-PDA-RVG group than Cy5.5-PDA group with broader fluorescence expression at all five time points (1 hour, 2 hours, 6 hours, 12 hours, and 24 hours). (**D**) Representative IVIS images of the brain and brain slices from AD mice at 24 hours post-injection revealed that PDA-RVG group had higher fluorescence intensity than PDA group. The color bar below Figure (**C** and **D**) indicates the fluorescence intensity, with yellow representing the highest and black the lowest intensity. (**E**) Hematology and blood biochemistry tests containing blood routine, liver and kidney function revealed no significant differences between the PDA-RVG and control groups, indicating PDA-RVG presented good biocompatibility.

equal slices according to the coronal plane. The PDA-RVG group also had the higher fluorescence intensity of brain tissue compared with PDA group (Figure 5D).

To evaluate the biocompatibility of PDA-RVG, mice were injected intravenously with normal saline or PDA-RVG every other day for one week, and then blood was collected for testing. Hematological analysis containing blood routine, liver and kidney function revealed no significant differences between the PDA-RVG and control groups, indicating that PDA-RVG presented good biocompatibility. (Figure 5E).

The Effect of PDA-RVG on Oxidative Stress and Inflammatory Response in vitro

The ROS scavenging effects of NPs are frequently determined by DCFH-DA fluorescent probe. Aβ42 stimulation significantly increased intracellular ROS levels in BV2 cells, which was inhibited by PDA or PDA-RVG treatment (Figure 6A).

https://doi.org/10.2147/IJN.S564013

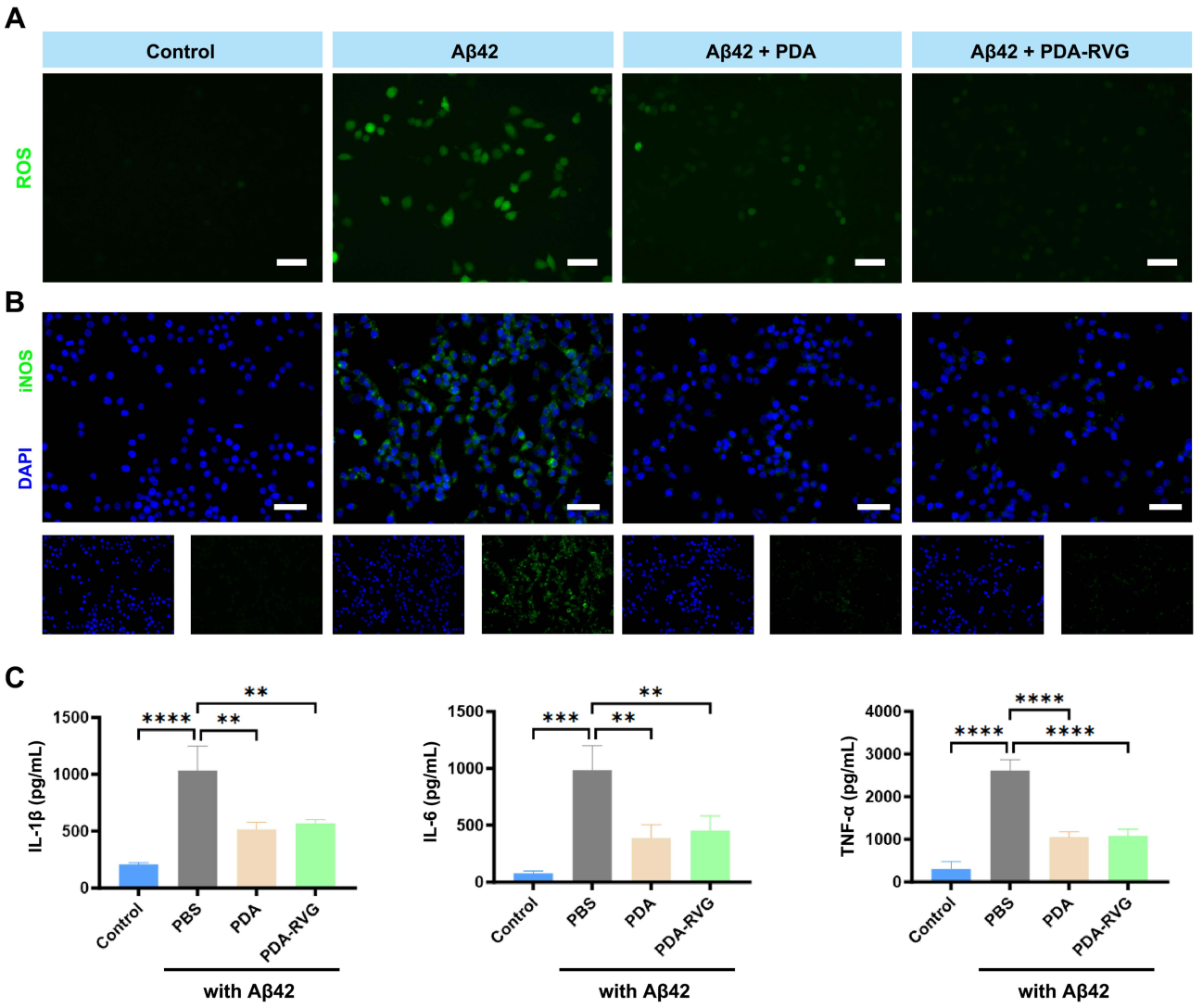

Figure 6 The effect of PDA-RVG on oxidative stress and inflammatory response in vitro. (**A**) Confocal microscopy images of BV2 cells stained with DCFH-DA showed that Aβ42 significantly increased intracellular ROS levels, which was inhibited by PDA or PDA-RVG treatment. Scale bar: 50 μm. (**B**) PDA or PDA-RVG treatment blocked the increase of iNOS (green) and DAPI (blue) double-labeled BV2 cells induced by Aβ42. Scale bar: 20 μm. (**C**) ELISA revealed that PDA or PDA-RVG treatment significantly reduced IL-1β, IL-6, and TNF-α levels compared with the Aβ42 group. $^{**}P<0.01$, $^{***}P<0.001$, $^{****}P<0.0001$.

Immunofluorescence staining showed that Aβ42 activated microglia and increased iNOS expression, and both PDA and PDA-RVG blocked the above effects (Figure 6B). In addition, we also detected the levels of pro-inflammatory cytokines IL-1β, IL-6, and TNF-α to evaluate the anti-inflammatory properties of PDA-RVG in vitro. Compared with Aβ42 group, PDA or PDA-RVG treatment significantly reduced IL-1β, IL-6, and TNF-α levels secreted by BV2 cells (Figure 6C).

The Cytoprotective Effects of the PDA-RVG in vitro

Dihydroethidium (DHE) probe was used as a ROS detector in this section. PC12 cells showed significantly increased intracellular DHE fluorescence signals after Aβ42 stimulation, which was attenuated by PDA or PDA-RVG treatment (Figure 7A).

Immunofluorescence results showed that intracellular GPX4 protein was decreased after Aβ42 administration, which was suppressed by PDA or PDA-RVG (Figure 7B). It indicates that PDA-RVG is capable of inhibiting cellular ferroptosis by clearing ROS and reducing the process of cellular lipid peroxidation.

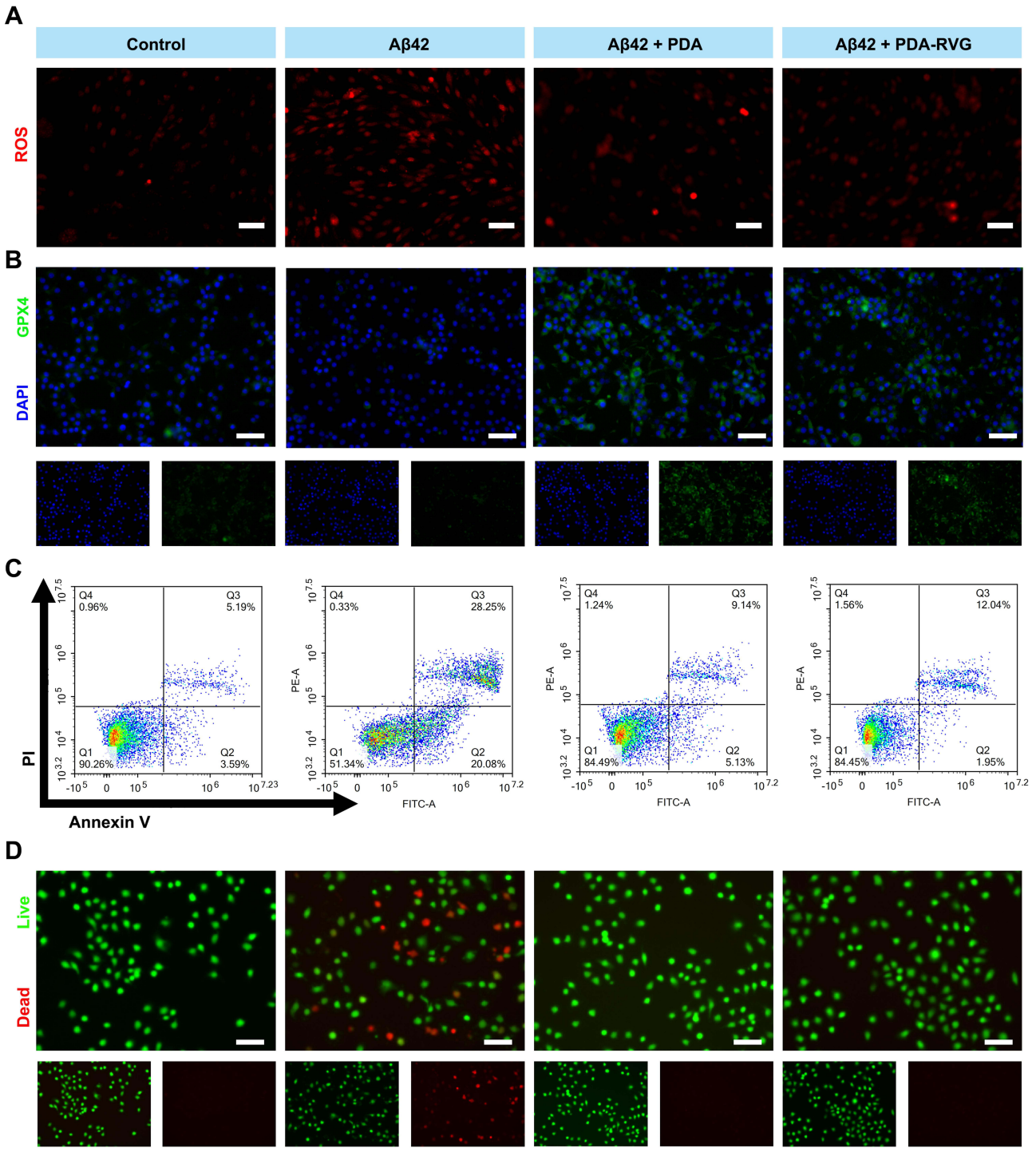

Figure 7 The cytoprotective effects of the PDA-RVG in vitro. (**A**) PC12 cells showed significantly increased intracellular ROS levels evaluated by DHE fluorescence signals after Aβ42 stimulation, which was attenuated by PDA or PDA-RVG treatment. Scale bar: 50 μm. (**B**) Immunofluorescence of GPX4 (green) and DAPI (blue) was decreased in Aβ42 group, which was suppressed by PDA or PDA-RVG. Scale bar: 50 μm. (**C**) PDA-RVG or PDA reduced Aβ42 inducing apoptotic PC12 cells assessed by staining with Annexin V-FITC and PI in flow cytometric analysis. (**D**) PDA or PDA-RVG significantly increased live PC12 cells stained with Calcein-AM (green) as well as decreased dead cells stained with PI (red). Scale bar: 50 μm.

We further performed quantitative analysis of apoptotic cells using flow cytometry, and the results displayed that Aβ42 increased the proportion of early and late apoptotic PC12 cells to 20.08% and 28.25%, respectively, while the proportion of healthy cells were decreased by 38.92%. PDA or PDA-RVG blocked Aβ42-induced apoptosis in PC12 cells, with the proportion of healthy cells increasing to 84.49% and 84.45%, respectively (Figure 7C).

https://doi.org/10.2147/IJN.S564013

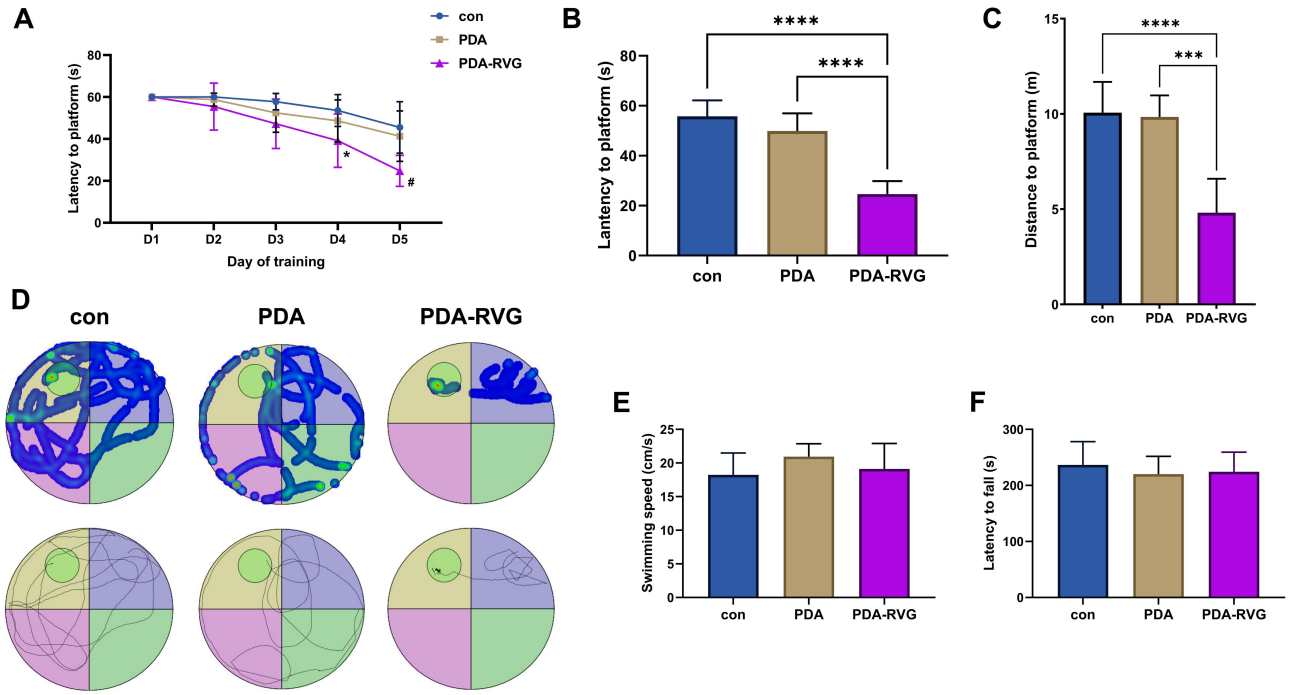

Figure 8 MWM evaluated the effect of PDA-RVG on cognitive function. The escape latency for locating the platform decreased in each group with more training trials, and PDA-RVG reduced the latency at 4 days and 5 days (**P*<0.05 vs control, # *P*<0.05 vs control and PDA) (**A**). PDA-RVG intravenous injection in the formal test on day 6 reduced the latency (**B**) and swimming distance (**C**) compared with the control and PDA groups, which was visually displayed in the trajectory map and heat map (**D**). The circle in the second quadrant represents the escape platform (**D**). No statistical differences in swimming speed (**E**) and fall latency in the Rotarod test (**F**) were revealed among the control, PDA, and PDA-RVG groups. ****P*<0.001, *****P*<0.0001.

Finally, after incubation with PDA or PDA-RVG for 8 hours, the viability of PC12 cells was assessed using Calcein AM/PI fluorescence staining. PDA or PDA-RVG significantly increased live PC12 cells and reduced dead cells induced by Aβ42, which may be due to the inhibition of the ROS accumulation and subsequent apoptosis by PDA (Figure 7D).

The Effect of PDA-RVG on Cognitive Function in APP/PS1 Mice

The escape latency during platform location decreased significantly in all groups with increased training trials in the MWM place navigation test, and the statistical difference between PDA-RVG and control and PDA groups started from day 4 ($P<0.05$) (Figure 8A). In the formal test on day 6, the mice subjected to PDA-RVG injection exhibited less latency and swimming distance than the control and PDA group, which was visually displayed in the trajectory map and heat map (Figure 8B–D). However, there was no statistical differences in swimming speed among the three groups (Figure 8E). The Rotarod test was used to assess mice's motor coordination and balance dysfunction,[38] and similar fall latency was revealed among the three groups (Figure 8F). The above results indicate PDA-RVG improved cognitive function independent of the impairment of vision and movement ability.

The Effect of PDA-RVG on Ferroptosis in APP/PS1 Mice

Western blot showed both FTH1 and GPX4 proteins were elevated by PDA-RVG (Figure 9A). Moreover, the *Fth1* gene was also increased, while the *Gpx4* gene displayed an unexpected decrease by PDA-RVG, which may be a negative feedback effect due to protein elevation (Figure 9B). It suggests that to exert the effect of anti-ferroptosis continuously, the administration of PDA-RVG may be further optimized, and maybe regular injection is a rational option.

Discussion

The current study demonstrated PDA was capable of improving cognitive function and reducing Aβ deposition in APP/PS1 mice. The modification of RVG29 granted intravenous delivery of PDA-RVG good brain-specific targeting ability

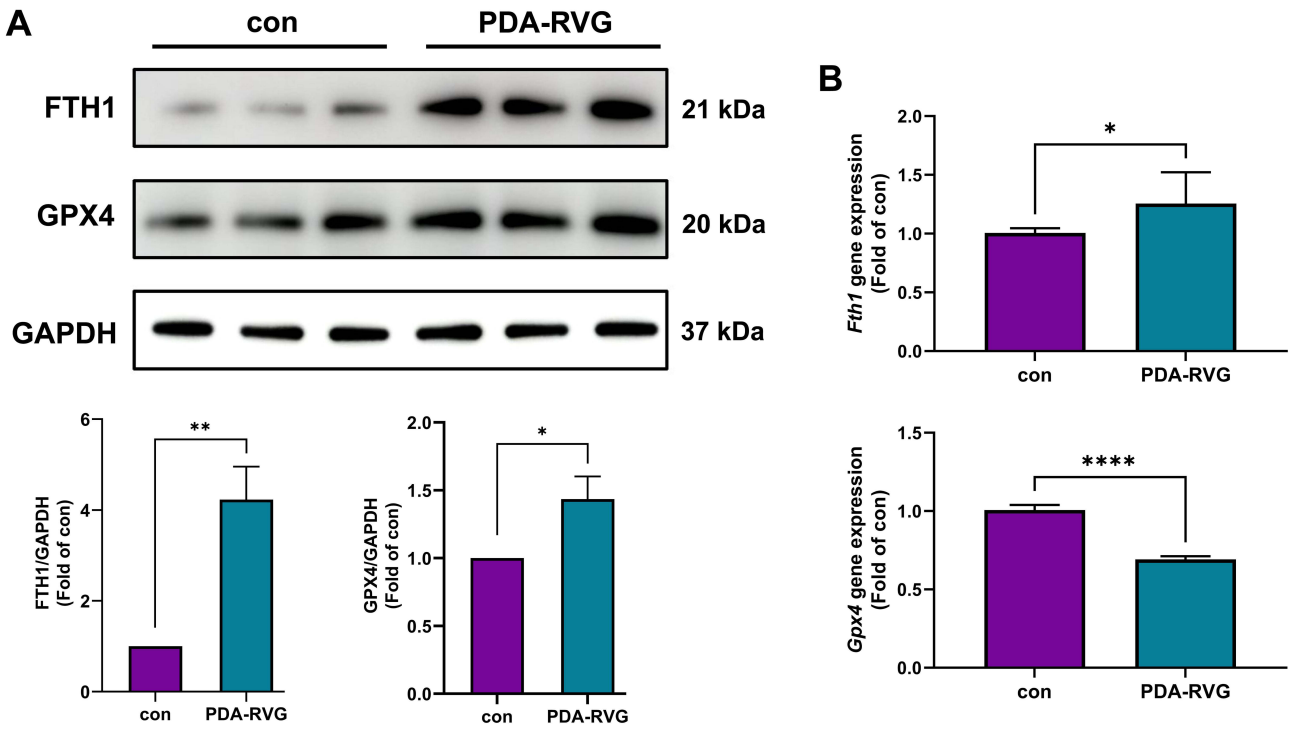

Figure 9 The effect of PDA-RVG on the expression of FTH1 and GPX4. (**A**) Both FTH1 and GPX4 proteins were elevated by intravenous injection of PDA-RVG in Western blot. **(B)** The *Fth1* gene was also increased, while the *Gpx4* gene expression was reduced by PDA-RVG. **P*<0.05, ***P*<0.01, *****P*<0.0001.

and biocompatibility. The mechanisms of treatment for AD included ameliorating oxidative stress and inhibiting inflammatory response and ferroptosis.

More and more evidence supports that NPs present promising potential use in treating AD, especially in reducing AD pathology.[39] For instance, gold NPs can reduce Aβ aggregation, scavenge ROS, inhibit neuroinflammation, influence neurotransmitter systems, and increase expression of neurotrophic factor in AD.[40] Similarly, previous studies have demonstrated PDA reduces Aβ burden, the mechanism of which includes the strong interaction of PDA with Aβ monomers/fibrils through its multiple recognition sites.[41] The results are in agreement with our findings in APP/PS1 transgenic mice, which are co-expressing a chimeric mouse/human APP and a mutant human PSEN1 and the most extensively utilized AD models. Both transgenes are implicated in early-onset familial AD, driving Aβ deposition and memory impairments that closely resemble human AD pathology.[42] As a result, this kind of transgenic mouse has detectable brain Aβ plaques, and their AD phenotypes get into a progressive stage during aging.[43] Since we had demonstrated PDA reduced Aβ burden, we further investigated the mechanisms by testing the expression of the two crucial proteins APP and PSEN1, and found they were significantly reduced by PDA. Interestingly, the *Psen1* gene appeared to have a "rebound" increase at 7 days, which may be explained by a negative feedback effect due to protein elevation. It also indicates that PDA's impact may not be long-lasting and weaken over time, which requires continuous administration. In addition, as the intracerebroventricular injection is invasive, a more convenient administration should be further investigated.

In order to conveniently deliver PDA to the brain intravenously, the RVG29 polypeptide derived from the RVG that can cross the BBB had been engineered and modified onto the surface of PDA. Expectably, we successfully demonstrated that intravenous delivery of PDA-RVG had good brain-specific targeting ability and biocompatibility. Importantly, PDA-RVG rather than PDA significantly improved cognitive function assessed by MWM, which is commonly used for assessing hippocampus-dependent spatial learning and long-term spatial memory of rodents.[44] This suggests that PDA-RVG improves cognition by crossing the BBB to elicit neuroprotective effects. Moreover, our data have indicated that both PDA and PDA-RVG can be regarded as an effective ROS scavenger. To determine whether the effective ROS-scavenging properties had reliable therapeutic effects, we examined the potential antioxidant and anti-inflammatory roles in both in vitro and in vivo models. Microglia are the primary immune cells in the brain and play a crucial role in the

https://doi.org/10.2147/IJN.S564013

initiation and development of AD.[45] Aβ42-stimulated BV2 cells are commonly used to evaluate in vitro inflammation in AD. Increased M1 microglia in the brains of AD mice can promote or maintain inflammatory responses by producing pro-inflammatory cytokines. Under pathological conditions, M1 microglia produce considerable amount of iNOS.[46] A great deal of NO produced by iNOS reacts with ·O2 to generate ·ONOO-, which damages tissues and promotes the development of AD. Therefore, the anti-inflammatory effect of PDA-RVG can be assessed by reducing the proportion of M1 microglia. In addition, the pro-inflammatory cytokines IL-1β, IL-6, and TNF-α also induce oxidative stress.[47] As a result, the findings indicate that PDA-RVG inhibits oxidative stress and inflammatory response by inhibiting activated microglia and reducing the levels of pro-inflammatory factors.

In AD pathology, ROS not only activate microglia and maintain the inflammatory microenvironment within the brain, but also directly act on neural cells to trigger cell death processes such as apoptosis and ferroptosis, resulting in neurological impairment. A sufficient accumulation of ROS triggers a series of apoptotic signals, forcing the cell to undergo programmed cell death.[48] Apoptosis-induced neuronal dysfunction leads to Aβ42 deposition and neurological dysfunction. Our work using Annexin V/PI detection and Calcein AM/PI fluorescence staining indicates PDA-RVG can help inhibit neuronal apoptosis, and the loading of RVG does not reduce its cytoprotective properties. In addition, ferroptosis is an iron-dependent form of programmed cell death driven by oxidative stress, playing a crucial role in the progression of AD.[49] FTH1 and GPX4 are two crucial ferroptosis-related proteins. FTH1 is one of the subunits of ferritin, which is responsible for rapid iron detoxification and can convert Fe^{2+} to Fe^{3+}.[50] A decrease in FTH1 aggravates oxidative stress and ferroptosis in the AD model.[51] Furthermore, GPX4 resists ferroptosis in cells by converting L-OOH into L-OH and then preventing the generation of lipid ROS. Also, activation of GPX4 can inhibit ferroptosis in AD.[52] As a result, we evaluated the effect of PDA-RVG on ferroptosis by observing the changes in two proteins. We demonstrated that PDA-RVG inhibited ferroptosis in both AD cell and animal models, suggesting it is also an important effect resulting from oxidative stress suppression.

The current study also has some limitations. First of all, although PDA-RVG protects against AD, this research is limited to animal experiments. The efficacy and safety of PDA-RVG in clinical translation should be further investigated. Polymeric NPs are biocompatible, US Food and Drug Administration-approved materials with the advantage of tunable drug release and easy surface functionalization.[53] As a result, PDA-RVG may be a promising drug for future clinical application. In addition, when examining the effect of PDA-RVG on oxidative stress in vivo, we had not compared with PDA alone.

Conclusion

In the current work, sufficient doses of PDA demonstrate the ability to scavenge ROS, ameliorate the inflammatory microenvironment and inhibit ferroptosis in vitro, and effectively reduce Aβ deposition in vivo. Modifying the RVG29 polypeptide grants intravenous delivery of PDA-RVG good brain-specific targeting ability and biocompatibility. Compared with PDA alone, intravenous delivery of PDA-RVG significantly improves cognitive function in AD mice. Disease modifying therapy is the future direction of AD treatment. However, a key challenge is the inefficiency of the drugs in crossing the BBB. Therefore, the development of NP delivery systems entails the encapsulation of active components and the exploitation of mechanisms such as transcytosis to achieve BBB penetration.[54] Besides, the nanomedicines are capable of alleviating AD pathology. As the findings of our study, we provide a safe, effective, and promising therapeutic strategy for AD via oxidative stress-associated target. It broadens the potential applications of the designed peptide-based brain-targeted drug delivery platform in the biomedical field.

Data Sharing Statement

Data will be made available on request from the corresponding author Lixian Jiang.

Ethical Approval

Our animal studies and protocol were approved by Institutional Animal Care and Use Committee of Shanghai Sixth People's Hospital Affiliated to Shanghai Jiao Tong University School of Medicine.

Author Contributions

All authors made a significant contribution to the work reported, whether that is in the conception, study design, execution, acquisition of data, analysis and interpretation, or in all these areas; took part in drafting, revising or critically reviewing the article; gave final approval of the version to be published; have agreed on the journal to which the article has been submitted; and agree to be accountable for all aspects of the work.

Funding

This research was supported by grants from the National Natural Science Foundation of China (No. 82071472; 81901102; 82171198).

Disclosure

The authors report no conflicts of interest in this work.

References

1. Nianogo RA, Rosenwohl-Mack A, Yaffe K, Carrasco A, Hoffmann CM, Barnes DE. Risk factors associated with alzheimer disease and related dementias by sex and race and ethnicity in the US. *JAMA Neurol*. 2022;79:584–91.
2. Chu H, Huang C, Xie F, Guo Q. The association between constipation and positron emission tomography and blood-based biomarkers in older cognitively unimpaired adults with higher amyloid-β burden. *Neurol Ther*. 2024;13:1701–1715. doi:10.1007/s40120-024-00666-x
3. Wagemann O, Liu H, Wang G, et al. Downstream biomarker effects of gantenerumab or solanezumab in dominantly inherited Alzheimer disease. *JAMA Neurol*. 2024;81:81. doi:10.1001/jamaneurol.2023.4387
4. Chu H, Huang C, Guan Y, Xie F, Chen M, Guo Q. The associations between nutritional status and physical frailty and Alzheimer's disease plasma biomarkers in older cognitively unimpaired adults with positive of amyloid-β PET. *Clin Nutr*. 2024;43:1647–1656. doi:10.1016/j.clnu.2024.05.024
5. Mintun MA, Lo AC, Duggan Evans C, et al. Donanemab in early Alzheimer's disease. *New Eng J Med*. 2021;384:1691–1704. doi:10.1056/NEJMoa2100708
6. van Dyck CH, Swanson CJ, Aisen P, et al. Lecanemab in early Alzheimer's disease. *New Eng J Med*. 2023;388:9–21. doi:10.1056/NEJMoa2212948
7. Jagust WJ, Teunissen CE, DeCarli C. The complex pathway between amyloid β and cognition: implications for therapy. *Lancet Neurol*. 2023;22:847–857. doi:10.1016/S1474-4422(23)00128-X
8. Pappolla MA, Martins RN, Poeggeler B, et al. Oxidative stress in Alzheimer's disease: the shortcomings of antioxidant therapies. *J Alzheimers Dis*. 2024;101:S155–S178. doi:10.3233/JAD-240659
9. Roy RG, Mandal PK, Maroon JC. Oxidative stress occurs prior to amyloid aβ plaque formation and tau phosphorylation in Alzheimer's disease: role of glutathione and metal ions. *ACS Chem Neurosci*. 2023;14:2944–2954. doi:10.1021/acschemneuro.3c00486
10. Bai R, Guo J, Ye X-Y, Xie Y, Xie T. Oxidative stress: the core pathogenesis and mechanism of Alzheimer's disease. *Ageing Res Rev*. 2022;77:101619.
11. Tang D, Chen X, Kang R, Kroemer G. Ferroptosis: molecular mechanisms and health implications. *Cell Res*. 2020;31:107–125. doi:10.1038/s41422-020-00441-1
12. Wu L, Xian X, Tan Z, et al. The role of iron metabolism, lipid metabolism, and redox homeostasis in Alzheimer's disease: from the perspective of ferroptosis. *Mol Neurobiol*. 2023;60:2832–2850. doi:10.1007/s12035-023-03245-7
13. Ehringer H, Hornykiewicz O. Distribution of noradrenaline and dopamine (3-hydroxytyramine) in the human brain and their behavior in diseases of the extrapyramidal system. *Parkinsonism Relat Disord*. 1998;4:53–57. doi:10.1016/S1353-8020(98)00012-1
14. Bohnen NI, Albin RL. The cholinergic system and Parkinson disease. *Behav Brain Res*. 2011;221:564–573. doi:10.1016/j.bbr.2009.12.048
15. Battaglini M, Emanet M, Carmignani A, Ciofani G. Polydopamine-based nanostructures: a new generation of versatile, multi-tasking, and smart theranostic tools. *Nano Today*. 2024;55:102151.
16. Jiang L, Zhang X, Wang S, et al. Functional monomers equipped microgel system for managing parkinson's disease by intervening chemokine axis-mediated nerve cell communications. *Adv Sci*. 2024;12:2410070.
17. Liu H, Qu X, Tan H, et al. Role of polydopamine's redox-activity on its pro-oxidant, radical-scavenging, and antimicrobial activities. *Acta Biomaterialia*. 2019;88:181–196. doi:10.1016/j.actbio.2019.02.032
18. Chen Y, Lv W, Xu J, et al. Mesenchymal stem cell membrane camouflaged mesoporous polydopamine for Parkinson's disease treatment via alleviating oxidative stress mediated neuroinflammation. *Biomaterials*. 2026;324:123537.
19. Huang Q, Jiang C, Xia X, et al. Pathological BBB crossing melanin-like nanoparticles as metal-ion chelators and neuroinflammation regulators against Alzheimer's disease. *Research*. 2023;6:0180.
20. Khan AR, Liu M, Khan MW, Zhai G. Progress in brain targeting drug delivery system by nasal route. *J Control Release*. 2017;268:364–389. doi:10.1016/j.jconrel.2017.09.001
21. Liu Z, Deng Q, Qin G, et al. Biomarker-activated multifunctional lysosome-targeting chimeras mediated selective degradation of extracellular amyloid fibrils. *Chem*. 2023;9:2016–2038. doi:10.1016/j.chempr.2023.06.003
22. Oswald M, Geissler S, Goepferich A. Targeting the Central Nervous System (CNS): a review of rabies virus-targeting strategies. *Mol Pharm*. 2017;14:2177–2196. doi:10.1021/acs.molpharmaceut.7b00158
23. Grove J, Marsh M. The cell biology of receptor-mediated virus entry. *J Cell Biol*. 2011;195:1071–1082. doi:10.1083/jcb.201108131
24. Schnell MJ, McGettigan JP, Wirblich C, Papaneri A. The cell biology of rabies virus: using stealth to reach the brain. *Nat Rev Microbiol*. 2009;8:51–61. doi:10.1038/nrmicro2260

25. Avila-Olias M, Pegoraro C, Battaglia G, Canton I. Inspired by nature: fundamentals in nanotechnology design to overcome biological barriers. *Ther Deliv*. 2012;4:27–43. doi:10.4155/tde.12.126
26. Sun C, Sha S, Shan Y, et al. Intranasal Delivery of BACE1 siRNA and berberine via engineered stem cell exosomes for the treatment of Alzheimer's disease. *I J Nanomed*. 2025;20:5873–5891. doi:10.2147/IJN.S506793
27. Li Z, Yang J, Li J, et al. Targeted delivery of BACE1 siRNA for synergistic treatment of Alzheimer's disease. *Transl Neurodegener*. 2025;14:14. doi:10.1186/s40035-025-00471-y
28. Jian C, Hong Y, Liu H, Yang Q, Zhao S. ROS-responsive quercetin-based polydopamine nanoparticles for targeting ischemic stroke by attenuating oxidative stress and neuroinflammation. *Int J Pharm*. 2025;669:125087.
29. Zhang Y, Ren X, Wang Y, et al. Targeting ferroptosis by polydopamine nanoparticles protects heart against ischemia/reperfusion injury. *ACS Appl Mater Interfaces*. 2021;13:53671–53682. doi:10.1021/acsami.1c18061
30. Yang Y, Wang Y, Jiang X, et al. Modified Ce/Zr-MOF nanoparticles loaded with curcumin for alzheimer's disease via multifunctional modulation. *Int J Nanomed*. 2024;19:9943–9959. doi:10.2147/IJN.S479242
31. Chu H, Yang X, Huang C, Gao Z, Tang Y, Dong Q. Apelin-13 protects against ischemic blood-brain barrier damage through the effects of aquaporin-4. *Cerebrovasc Dis*. 2017;44:10–25. doi:10.1159/000460261
32. Chu H, Ding H, Tang Y, Dong Q. Erythropoietin protects against hemorrhagic blood–brain barrier disruption through the effects of aquaporin-4. *Lab Invest*. 2014;94:1042–1053. doi:10.1038/labinvest.2014.84
33. Chu H, Dong J, Tang Y, Huang C, Guo Q. Connexin 43 promotes neurogenesis via regulating aquaporin-4 after cerebral ischemia. *Neurotox Res*. 2023;41:349–361. doi:10.1007/s12640-023-00646-3
34. Xie R, Zhao W, Lowe S, et al. Quercetin alleviates kainic acid-induced seizure by inhibiting the Nrf2-mediated ferroptosis pathway. *Free Radic Biol Med*. 2022;191:212–226. doi:10.1016/j.freeradbiomed.2022.09.001
35. Kaufman AC, Salazar SV, Haas LT, et al. Fyn inhibition rescues established memory and synapse loss in Alzheimer mice. *Ann Neurol*. 2015;77:953–971. doi:10.1002/ana.24394
36. Huang C, Chu H, Ma Y, et al. The neuroprotective effect of deep brain stimulation at nucleus basalis of Meynert in transgenic mice with Alzheimer's disease. *Brain Stimul*. 2019;12:161–174. doi:10.1016/j.brs.2018.08.015
37. Park M, Ha J, Lee Y, Choi H-S, Kim BS, Jeong YK. Low-moderate dose whole-brain γ-ray irradiation modulates the expressions of glial fibrillary acidic protein and intercellular adhesion molecule-1 in the 1-methyl-4-phenyl-1,2,3,6-tetrahydropyridine–induced Parkinson's disease mouse model. *Neurobiol Aging*. 2023;132:175–184. doi:10.1016/j.neurobiolaging.2023.06.015
38. Yuan C, Shi L, Sun Z, et al. Regulatory T cell expansion promotes white matter repair after stroke. *Neurobiol Dis*. 2023;179:106063.
39. Koga-Batko J, Antosz-Popiołek K, Nowakowska H, et al. Nanoparticles as an encouraging therapeutic approach to Alzheimer's disease. *Int J Mol Sci*. 2025;27:26. doi:10.3390/ijms27010026
40. Sivamaruthi BS, Kesika P, Sisubalan N, Chaiyasut C. Advances in gold nanoparticles for the diagnosis and management of Alzheimer's disease. *Pharmaceutics*. 2025;18:17. doi:10.3390/pharmaceutics18010017
41. Yin Z, Zhang Z, Gao D, et al. Stepwise coordination-driven metal–phenolic nanoparticle as a neuroprotection enhancer for Alzheimer's disease therapy. *ACS Appl Mater Interfaces*. 2022;15:524–540. doi:10.1021/acsami.2c18060
42. Liu Y, Xu YF, Zhang L, et al. Effective expression of Drebrin in hippocampus improves cognitive function and alleviates lesions of Alzheimer's disease in APP (swe)/PS1 (ΔE9) mice. *CNS Neurosci Ther*. 2017;23:590–604. doi:10.1111/cns.12706
43. Yan P, Bero AW, Cirrito JR, et al. Characterizing the appearance and growth of amyloid plaques in APP/PS1 mice. *J Neurosci*. 2009;29:10706–10714. doi:10.1523/JNEUROSCI.2637-09.2009
44. Ye M, Chung H-S, An YH, et al. Standardized herbal formula PM012 decreases cognitive impairment and promotes neurogenesis in the 3xTg AD mouse model of Alzheimer's disease. *Mol Neurobiol*. 2015;53:5401–5412. doi:10.1007/s12035-015-9458-x
45. Geng F, Zhao N, Ren Q. Circadian rhythm, microglia-mediated neuroinflammation, and Alzheimer's disease. *Neurosci Biobehav Rev*. 2025;170.
46. Xu Z, Zhu M, Xie H, et al. SIX1 aggravates the progression of spinal cord injury in mice by promoting M1 polarization of microglia. *Scie Rep*. 2025;15.
47. Woods C, Wang G, Milner TA, Glass MJ. Tumor necrosis factor alpha induces NOX2-dependent reactive oxygen species production in hypothalamic paraventricular nucleus neurons following angiotensin II infusion. *Neurochem Int*. 2024;179.
48. Trofin D-M, Sardaru D-P, Trofin D, et al. Oxidative stress in brain function. *Antioxidants*. 2025;15:14. doi:10.3390/antiox15010014
49. Hao Z, Guo X, Wu J, Yang G. Revisiting the benefits of exercise for alzheimer's disease through the lens of ferroptosis: a new perspective. *Aging Dis*. 2024;16:3268–3283. doi:10.14336/AD.2024.1560
50. Yang L, Zhang M, Liu M, et al. Loss of FTH1 induces ferritinophagy-mediated ferroptosis in anaemia of myelodysplastic syndromes. *J Cell Mol Med*. 2025;29. doi:10.1111/jcmm.70350
51. Thompson K, Menzies S, Muckenthaler M, et al. Mouse brains deficient in H-ferritin have normal iron concentration but a protein profile of iron deficiency and increased evidence of oxidative stress. *J Neurosci Res*. 2002;71:46–63. doi:10.1002/jnr.10463
52. Yong Y, Yan L, Wei J, et al. A novel ferroptosis inhibitor, Thonningianin A, improves Alzheimer's disease by activating GPX4. *Theranostics*. 2024;14:6161–6184. doi:10.7150/thno.98172
53. Nájera-Maldonado L, Parra-González M, Peralta-Cuevas E, Gutierrez-Onofre AJ, Garcia-Atutxa I, Villanueva-Flores F. Cracking the blood–brain barrier code: rational nanomaterial design for next-generation neurological therapies. *Pharmaceutics*. 2025;18:17.
54. Kshirsagar N, Patil A, Suryawanshi M. Bioactive compound nanoparticles for Alzheimer's disease. *Inflammopharmacology*. 2025;33:2963–2976. doi:10.1007/s10787-025-01801-2